Int J Earth Sci (Geol Rundsch) (2017) 106:2371–2386
DOI 10.1007/s00531-016-1432-y

ORIGINAL PAPER

Variable anelastic attenuation and site effect in estimating source parameters of various major earthquakes including M_w 7.8 Nepal and M_w 7.5 Hindu kush earthquake by using far-field strong-motion data

Naresh Kumar[1] · Parveen Kumar[1] · Vishal Chauhan[1] · Devajit Hazarika[1]

Received: 30 September 2016 / Accepted: 30 November 2016 / Published online: 22 December 2016

Abstract Strong-motion records of recent Gorkha Nepal earthquake (M_w 7.8), its strong aftershocks and seismic events of Hindu kush region have been analysed for estimation of source parameters. The M_w 7.8 Gorkha Nepal earthquake of 25 April 2015 and its six aftershocks of magnitude range 5.3–7.3 are recorded at Multi-Parametric Geophysical Observatory, Ghuttu, Garhwal Himalaya (India) >600 km west from the epicentre of main shock of Gorkha earthquake. The acceleration data of eight earthquakes occurred in the Hindu kush region also recorded at this observatory which is located >1000 km east from the epicentre of M_w 7.5 Hindu kush earthquake on 26 October 2015. The shear wave spectra of acceleration record are corrected for the possible effects of anelastic attenuation at both source and recording site as well as for site amplification. The strong-motion data of six local earthquakes are used to estimate the site amplification and the shear wave quality factor (Q_β) at recording site. The frequency-dependent $Q_\beta(f) = 124f^{0.98}$ is computed at Ghuttu station by using inversion technique. The corrected spectrum is compared with theoretical spectrum obtained from Brune's circular model for the horizontal components using grid search algorithm. Computed seismic moment, stress drop and source radius of the earthquakes used in this work range 8.20×10^{16}–5.72×10^{20} Nm, 7.1–50.6 bars and 3.55–36.70 km, respectively. The results match with the available values obtained by other agencies.

✉ Parveen Kumar
sainiparveen.saini@gmail.com

[1] Wadia Institute of Himalayan Geology, 33 GMS Road, Dehradun 248001, India

Keywords Strong motion · Gorkha Nepal earthquake · Hindu kush earthquake · Seismic moment · Stress drop

Introduction

The Himalayan region is complex on account of tectonic deformation and geological set-up due to the ongoing India–Eurasia collision since ~55 Ma (Yin 2006; Muller 2010; Mukherjee 2005, 2013; Jain 2014; Mukherjee et al. 2013, 2015). In the past, the region has witnessed natural disasters such as devastating earthquakes. Well-documented and instrumentally recorded events in the Himalaya include 1887 Shillong, 1905 Kangra, 1934 Bihar, 1950 Assam and 2005 Muzaffarabad earthquake. The recent shallow focused Gorkha Nepal earthquake (M_w 7.8 of 25 April 2015) and intermediate depth focused Hindu kush earthquake (M_w 7.5 of 26 October 2015) are the events of same extent occurred in the central and western part of the Himalaya, respectively (Fig. 1). The 15-km-deep Gorkha Nepal earthquake has caused a widespread destruction and casualties of over 8500 in Nepal (Bilham 2015) and also in nearby regions. The earthquake was followed by several $M > 5.0$ large size aftershocks. The aftershock occurred on 12 May 2015 is the largest event with M_w 7.3. Figure 1 presents the epicentres of main shock and large size aftershocks. The recent Hindu kush earthquake of M_w 7.5 occurred on 26 October 2015 is the largest earthquake of Hindu kush region (Fig. 1) within the western edge of the Himalayan belt during last 10 years. The Hindu kush region is one of the world's most seismically active areas where most of the earthquakes occur at 70–300 km intermediate focal depth (Pavlis 2000). Due to intermediate focal depth, the recent earthquake in this region was not so severe; however, it has shattered different parts of

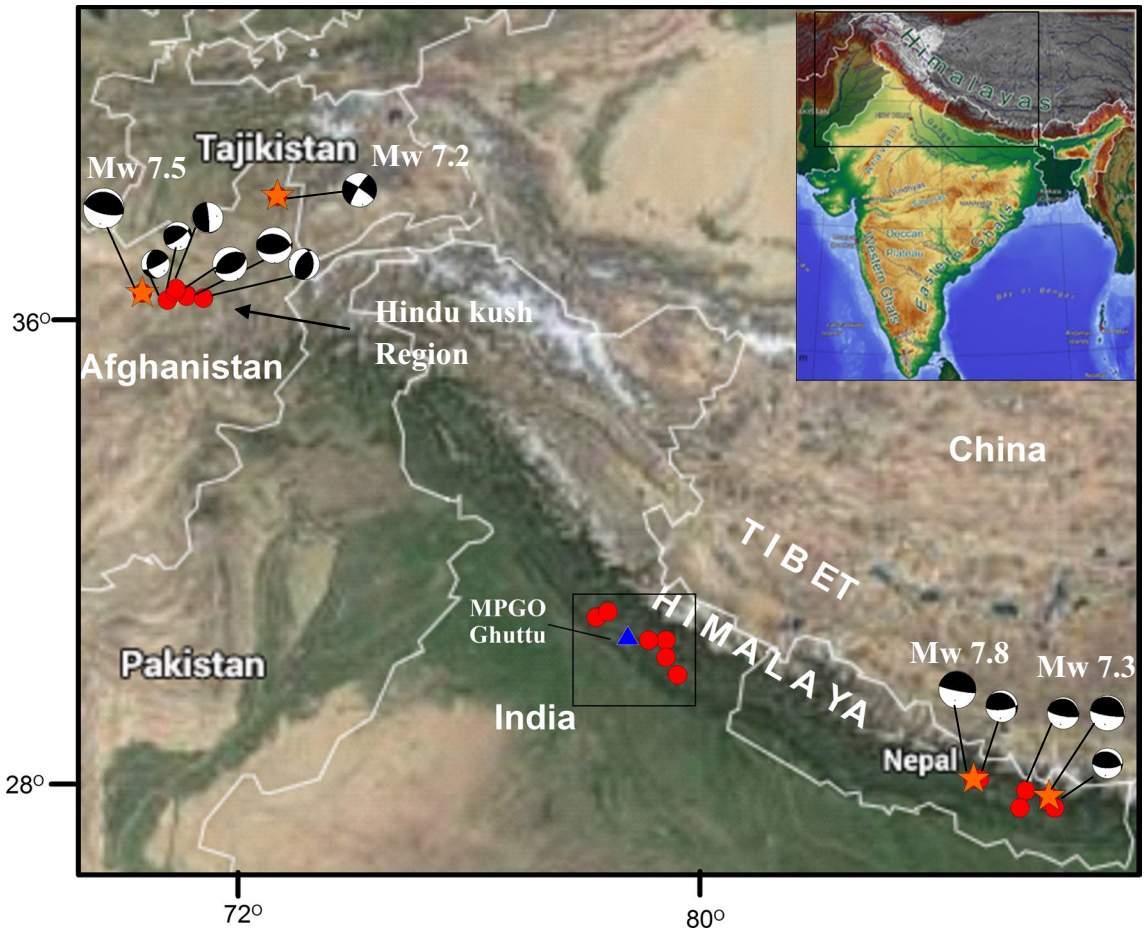

Fig. 1 Location of recording station, epicentres of local events, Hindu kush region earthquakes, Gorkha Nepal earthquake and its aftershocks. Epicentres of major events (M_w > 7.0) are marked with *orange star* and other earthquakes with *red circle*. Focal mechanisms extracted from USGS Harvard CMT solutions of M > 5.3 are shown with lower hemisphere beach balls

surrounding countries, i.e. Afghanistan, Pakistan, India and Tajikistan. The recent Nepal and Hindu kush earthquakes and their corresponding strong aftershocks with magnitude range 5.2–7.3 were recorded at Ghuttu accelerograph station (30.53°N, 78.74°E and 1868 m altitude) situated in Garhwal Himalaya, Uttarakhand, India.

The strong-motion data are utilized to investigate the attenuation and site effects of region during the occurrence of major and higher magnitude earthquakes. The far-field records are also utilized for calculation of source parameters (e.g. seismic moment, rupture source radius and the stress drop) of large magnitude earthquake (Kanamori 1979; Irikura 1983). These parameters are evaluated based on the circular source model of Brune (1970) and following Aki (1967). Recent advancement of digital recording system has assisted for the improvement in mathematical computing and relating the waveform spectra to different earthquake source parameters (Hanks 1977; Hanks and Kanamori 1979; Fletcher 1980, 1982). The high-frequency acceleration spectra generated at the source are modified along the propagation path and recording site. The amplitude decays as frequency rises. Therefore, at the recording site, the acceleration spectra are corrected for the diminution function to evaluate source parameters. The diminution function or decaying amplitude accounts to the geometrical spreading and anelastic attenuation term (Joshi et al. 2014), which are to be corrected at recording site. The anelastic attenuation is measured through shear wave quality factor, which plays an important role for the acceleration spectrum at large epicentre distance.

In the present work, source parameters of earthquakes in Nepal and Hindu kush region are estimated based on variable attenuation and site effects. The strong-motion data recorded by accelerograph station at Ghuttu, Garhwal Himalaya, at far-field distance are used, and the recording station situates in the west to the epicentres of earthquakes from Nepal region and to the east from Hindu kush region. In strong motion data, peak ground acceleration is associated with S-phase (Hadley et al. 1982; Kumar et al. 2013b, 2014b); therefore in this work, S-phase is utilized

to estimate source parameters of various earthquakes. The inversion technique proposed by Joshi (2006) and latter modified by Joshi et al. (2012) and Kumar et al. (2015) is used to estimate $Q_\beta(f)$ and site effects at recording station, and these values are further used to correct the observed spectrum. The spectrum is corrected for anelastic attenuation for both at the site and the source region. The computed $Q_\beta(f)$ value at recording station is used to correct the spectrum for site region, and $Q_\beta(f)$ values provided by various other workers for source region, i.e. Nepal region and Hindu kush region, are utilized to correct the spectrum for source region. The final corrected spectrum is compared with theoretical Brune's spectrum by using grid search method which provides various source parameters of the earthquakes used in this work.

Strong-motion data and earthquake source information

Wadia Institute of Himalayan Geology (WIHG), Dehradun, India, has installed a strong-motion recorder (accelerograph) at Ghuttu (India) station (Kumar and Khandelwal 2015). The Multi-Parametric Geophysical Observatory (MPGO) observatory lies over the Garhwal Lesser Himalaya, very close to the Vaikrita Thrust, a local tectonic name of the Main Central Thrust (MCT) (Mukherjee and Koyi 2010). The Garhwal Lesser Himalaya is comprised of fossiliferous Riphean sediments and in general covered by vast low- to medium-grade metamorphic rocks (Valdiya 1980). The region surrounding to the station belongs to Rautgara Formation of Lesser Himalaya that consists predominately quartzite comprising shale, slates and metavolcanic rocks (Islam and Thakur 1998; Vyshnavi et al. 2014). The accelerograph is a part of ten another geophysical instruments installed at single station under the MPGO for earthquake precursory studies. The accelerograph is located at a distance more than 600 km in the west from the rupture zone of M_w 7.8 Gorkha Nepal earthquake (Fig. 1). The Hindu kush earthquake of 26 October 2015 is located ~1000 km west of this station (Fig. 1). The station is equipped with MS2004+ force-balance accelerometer of SYSCOM instruments, Switzerland, which was installed in 2007. It is force feedback triaxial accelerometer having >500 Hz natural frequency. Its amplitude frequency response ranges up to 150 Hz with dynamic range of 110 dB and can measure ±1 g gravity variation. The 16-bit instrument records the strong-motion data in trigger mode at a sampling rate of 200 samples per second (Kumar and Khandelwal 2015).

The six local events having hypocentral distance between 36 and 109 km from MPGO are used to calculate $Q_\beta(f)$ and site effects at this station. The location and waveform record of these local events are shown in Fig. 2. The raw data collected from the accelerograph are corrected for baseline correction and instrument response based on the procedure described by Boore and Bommer (2005). In order to record strong and bigger size (M ≥ 6.0) earthquake from any part of the Himalaya, the trigger threshold of the accelerometer is kept at very low level of 0.245 mg. It has nicely recorded the temporal variation of acceleration during the occurrence of this recent Gorkha Nepal earthquake of 25 April 2015 and its large size aftershocks and bigger size (M ≥ 5.2) earthquakes from Hindu kush region. Detailed information of these events is given in Table 1, and the horizontal components of waveform records of five seismic events from the Nepal region and four events from the Hindu kush region are plotted in Fig. 3. The focal mechanisms of thirteen events of these earthquakes are extracted from USGS Centroid Moment Tensor (CMT) solutions and plotted in Fig. 1. Except one, all these events have caused thrust/reverse displacement on the rupture fault; however, none has extended up to earth's surface. Among these, the largest and shallow focused M_w 7.8 Gorkha Nepal earthquake has ruptured an upper crustal section between 5 and 15 km depth (Elliott et al. 2016; Whipple et al. 2016). A shallow focused major event (M_w 7.2) has pure strike slip motion of the rupture fault which is located in the northeast of Hindu kush within Tibetan plateau and to the north of western Himalayan syntaxes. Shallow focused seismic events of eastern Nepal region show thrust mechanism located on the Main Himalayan Thrust (MHT) causing thrusting of Indian plate under the Himalayan wedge and Eurasian plate. Seven events of intermediate focal depth of the Hindu kush region have thrust/reverse focal mechanisms with variable strike directions. The focal depth of these events is also variable, and it is supposed that the seimogenesis of this part is related to the subducted slab of the mantle of the Indian tectonic plate. The past and recent seismic activity reports intermediate depth earthquakes occurring in a slab of lithosphere hanging in the mantle (Chatelain et al. 1980; Roecker et al. 1980; Yadav et al. 2013; Ali and Shanker 2016).

Methodology

The acceleration spectra of the shear wave are analysed to calculate the earthquake source parameters. In the present work, acceleration spectra '$A(f)$' at a hypocentral distance R can be computed by the following formula (Boore 1983; Atkinson and Boore 1998):

$$A(f) = D(f)S_A(f) \quad (1)$$

where the terms $D(f)$ and $S_A(f)$ represent diminution function and source acceleration spectra, respectively. The diminution function is the resultant of geometrical spreading

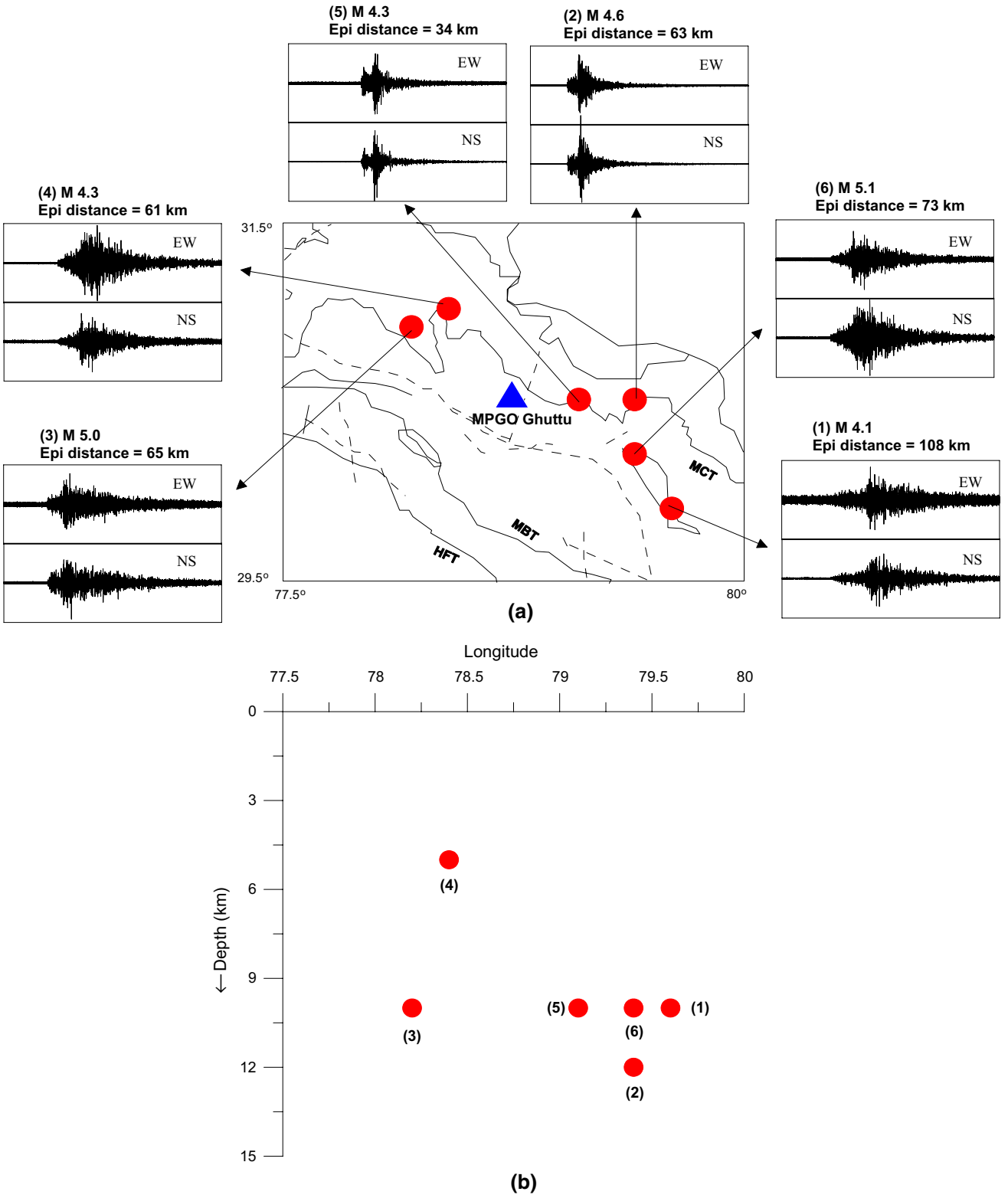

Fig. 2 **a** NS and EW component of acceleration records of six local seismic events recorded at MPGO Ghuttu station, **b** depth of the events corresponding to their epicentres. Marked event number is based on Table 1 of local events near recording station. *Circle* and *triangle* represent location of event and recording station, respectively. The tectonic features of the region are marked after Valdiya (1980)

Table 1 Origin time and information of the events used in the present study

SN.	Date (dd-mm-yyyy)	Origin time (hh:mm:s)	Lat. (°)	Long. (°)	Depth (km)	Magnitude	Source
Local events located close to recording station							
1	10-07-2010	03:16:20	29.9	79.6	10	4.1	India Meteorological Department (IMD)
2	20-06-2011	06:27:18	30.5	79.4	12	4.6	
3	09-02-2012	19:17:29	30.9	78.2	10	5.0	
4	11-02-2013	10:48:55	31.0	78.4	05	4.3	
5	06-04-2013	22:29:31	30.5	79.1	10	4.3	
6	01-04-2015	21:23:54	30.2	79.4	10	5.1	
Earthquakes occurred in Nepal and Hindu kush (Afghanistan) region							
1	25-04-2015	06:11:26	28.1	84.7	15	7.8	United States Geological Survey (USGS)
2	25-04-2015	06:45:21	28.1	84.8	14.6	6.6	
3	25-04-2015	06:56:05	27.9	85.6	10	5.5	
4	25-04-2015	08:55:56	27.6	85.5	10	5.3	
5	26-04-2015	07:09:10	27.7	86.0	17.3	6.7	
6	12-05-2015	07:05:19	27.8	86.0	15	7.3	
7	12-05-2015	07:36:53	27.6	86.1	15	6.3	
8	26-10-2015	09:09:42	36.5	70.3	231	7.5	
9	22-11-2015	18:16:04	36.4	71.4	102	5.7	
10	07-12-2015	07:50:05	38.2	72.7	22	7.2	
11	25-12-2015	19:14:47	36.4	71.1	206	6.3	
12	02-01-2016	08:37:22	36.5	70.9	189	5.2	
13	12-01-2016	20:04:59	36.5	70.9	239	5.7	
14	21-02-2016	09:12:08	36.4	70.8	174	5.2	
15	10-04-2016	10:28:58	36.4	71.1	212	6.6	

and anelastic attenuation along the wave propagation path which is described by Boore and Atkinson (1987) as given below:

$$D(f) = [e^{-\pi f R/Q_\beta(f)\beta} G(R)]P(f, f_m) \quad (2)$$

The terms $P(f, f_m)$ and $G(R)$ represent high-cut filter and geometrical spreading, respectively. The function $e^{-\pi f R/Q\beta(f)\beta}$ denotes anelastic attenuation, in which the terms R, $Q_\beta(f)$ and β denote hypocentral distance, frequency-dependent shear wave quality factor and shear wave velocity, respectively. Source acceleration spectrum is computed by using Eq. (1):

$$S_A(f) = A(f)/D(f) \quad (3)$$

The earthquake source size equivalent to rupture area can be expressed by seismic moment (M_o). In the present work, corner frequency (f_c) and long-term flat level (Ω_0) obtained from spectra of recorded data are used to determine the seismic moment which is expressed as (Brune 1970, 1971):

$$M_o = 4\pi\rho\beta^3\Omega_o R/FS\,R_{\theta\varphi} \quad (4)$$

In this equation, the terms ρ, β, FS and $R_{\theta\varphi}$ are density, velocity of S-wave, free surface effect and radiation pattern coefficient, respectively. The density and velocity of S-wave are considered as 2700 kg/m^3 and 3.5 km/s, respectively. The '$R_{\theta\varphi}$' is considered as 0.63 for shear wave (Atkinson and Boore 1995). The source radius (r_o) is defined as the radius of circular crack of rupture and is significant to model for obtaining earthquake source parameters. The expression relating source radius with the corner frequency (Brune 1970, 1971) of the recorded spectra is expressed as:

$$r_o = 2.34\beta/2\pi f_c \quad (5)$$

Stress drop ($\Delta\sigma$) is another important source parameter of an earthquake. Stress drop is defined as difference of shear stress on fault rupture zone before and after the occurrence of earthquake event (Ruff 1999). To evaluate a complete stress release from earthquake event, the stress drop can be calculated from seismic moment and the source radius using the expression given below (Papageorgiou and Aki 1983):

$$\Delta\sigma = 7M_o/16r_o^3 \quad (6)$$

As stated above, the recording station lies far away from the source region, and therefore, source and site region may have different attenuation characteristics. Therefore, in the

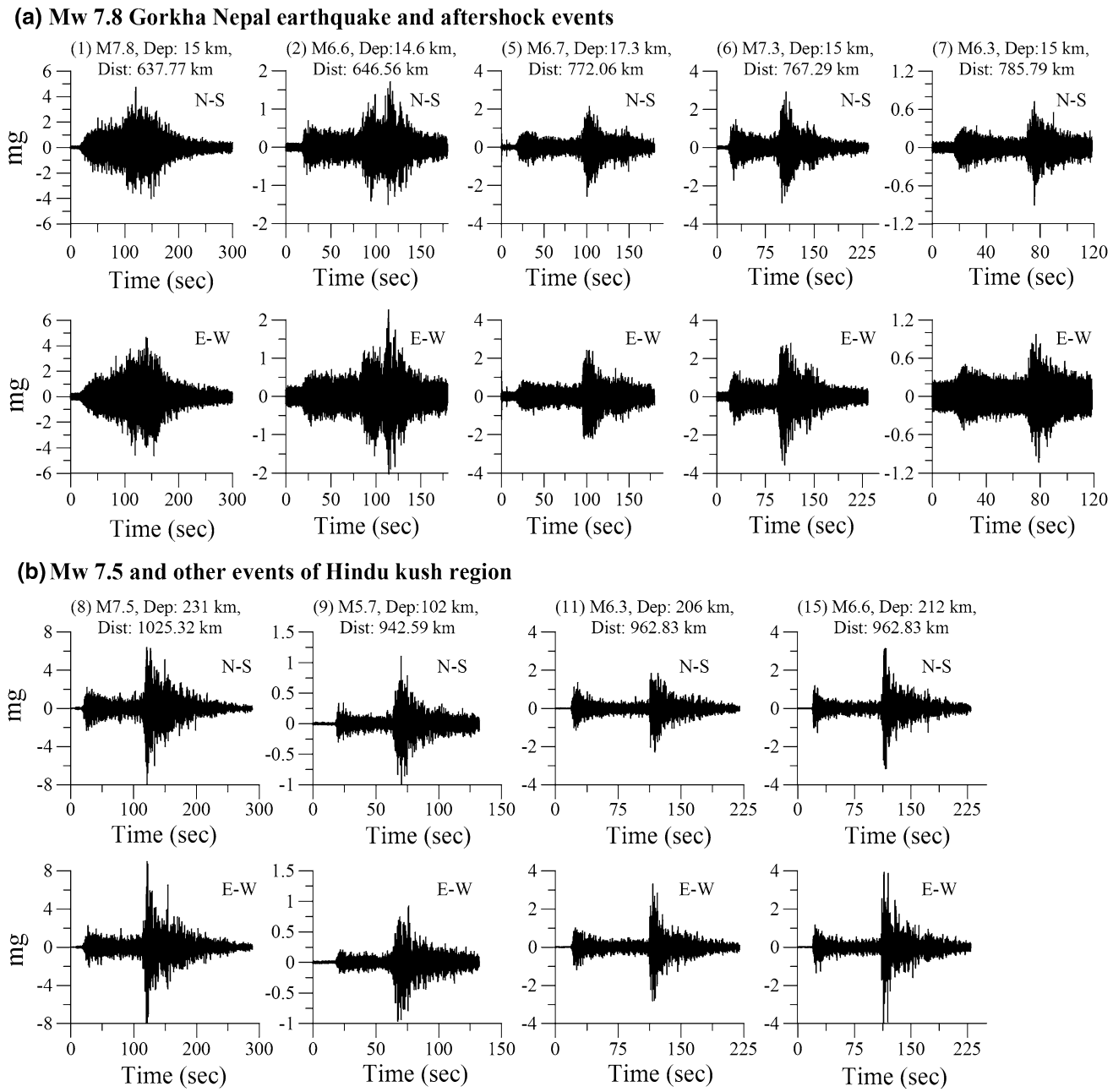

Fig. 3 Acceleration records of NS and EW components of strong and higher magnitude earthquakes of five events from the Nepal region (M_w 7.8 Gorkha Nepal earthquake and its aftershocks) and four events from the Hindu kush region. Marked event number is based on Table 1 which has detailed information of earthquake sources

present work, variable attenuation relations are used to correct the spectra. Separate values of quality factors are used for source and site regions. Hence, the following relation is used to compute the diminution function (Joshi et al. 2014):

$$D(f) = \exp\left[-\pi f\left(\frac{R-100}{Q_{\beta 2}.\beta_2} + \frac{100}{Q_{\beta_1}.\beta_1}\right)\right] \quad (7)$$

$Q_{\beta 1}$ and $Q_{\beta 2}$ are the quality factors of source and recording site regions, respectively where β_1 and β_2 are the s-wave velocities of these two regions, respectively. Therefore, in the present work, the region less than 100 km of hypocentral distance is considered as source region and that with hypocentral distance greater than 100 km is considered as site region. The quality factor value $Q_\beta(f) = 167f^{0.47}$ is used for the source region of eastern Nepal considered for the earthquakes occurred in Nepal region, which is taken from Nath et al. (2005) and Nath and Thingbaijam (2009). The $Q_\beta(f) = 130f^{0.79}$ and $Q_\beta(f) = 500$ are used for the source

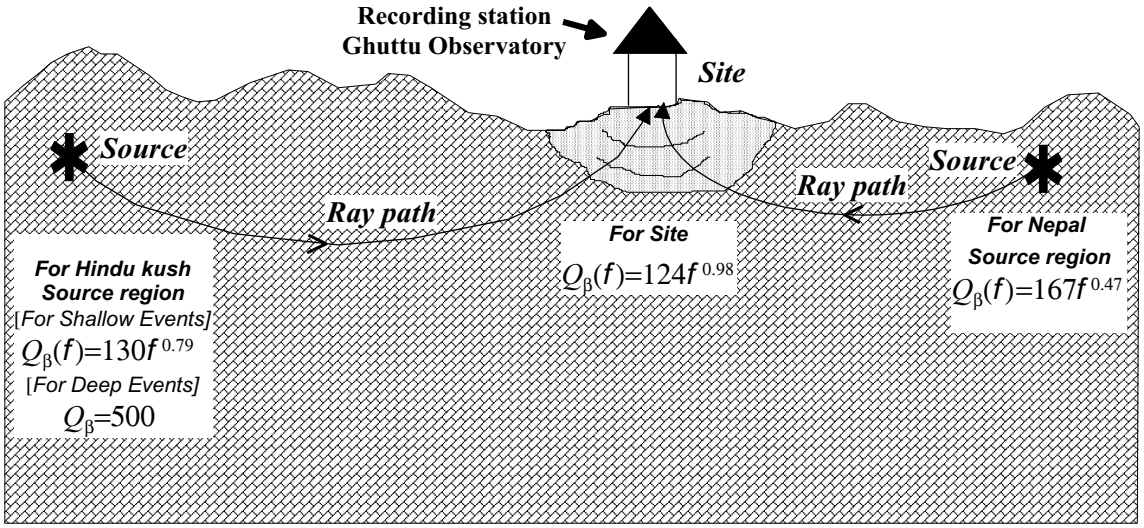

Fig. 4 Projection of ray path from source to recording station. Different $Q_\beta(f)$ value used for site region, source region of Hindu kush and source region of Nepal

region of Hindu kush to evaluate source parameters for the earthquakes occurred in Hindu kush region (Wu and Aki 1988; Yu et al. 1995). The wave propagation path and the characterization of regional attenuation properties are shown in Fig. 4 with a schematic diagram. In the data set of Hindu kush region, only one earthquake is shallow focused located in the upper most crust while the remaining events are of deeper origin with intermediate focal depth. Therefore, two separate Q_β values are considered for the Hindu kush source region. The quality factor and site effect used for the site region are computed by using the inversion technique. In the present work, time window covering complete S-phase is used to generate the spectrum and this spectrum is further used to estimate various source parameters. The window is cosine tapered and taken as 10% tapering for both ends (Sharma and Wason 1994). The FFT algorithm is used to obtain spectrum of acceleration time series, and the resultant spectrum is corrected for variable attenuation factors and site effect.

The obtained corrected spectra are finally used to estimate various source parameters. For this estimation, a comparison is made between the obtained corrected spectra and theoretical spectra (Brune 1970) by using the grid search method. Grid Search algorithm is used to minimize the misfit error functions between the observed and theoretical spectra. In this method, a number of possibilities of Ω_o and f_c are considered for estimation of Brune's theoretical spectrum. The best match of Brune's theoretical spectrum with the obtained spectrum of recorded data is selected based on minimum error, which provides the required values of Ω_o and f_c. The comparison is used to estimate seismic moment, stress drop and source radius by using the above-mentioned relations proposed by Brune (1970, 1971) and Papageorgiou and Aki (1983). In grid search method, a number of possibilities of Ω_o and f_c are tested to get best-fit theoretical spectrum with observed spectrum. Several iterations are performed, and root mean square error (RMSE) is computed for each iteration. The final values are selected corresponding to the iteration, which gives minimum RMSE as shown in Fig. 5. In this method, computation is started with the initial value of Ω_o and f_c, considered from the visual inspection of the obtained spectrum. For each additional iteration, the Ω_o and f_c are changed with an increment of 0.001. The best-fit spectrum is selected on the basis of minimum RMSE value.

Determination of shear wave quality factor and site effect

The local events recorded in Ghuttu region of Garhwal Himalaya, India, are utilized to estimate the $Q_\beta(f)$ and site effect at recording station. To determine these two parameters, strong-motion data of six local events (Table 1) are used, which have magnitude range 4.1–5.1. The inversion technique proposed by Joshi (2006) and later modified by Joshi et al. (2012) and Kumar et al. (2015) is used to obtain site effect and $Q_\beta(f)$. In this technique, the acceleration spectra A(f) can be computed as (Boore 1983 and Atkinson and Boore 1998):

$$A(f) = C\,S(f)\,D(f) \tag{8}$$

where 'C' is the constant term, and '$S(f)$' and '$D(f)$' are the source spectra and diminution function, respectively. The diminution function is described by Eq. (2) in which the term C is constant for a particular station for an earthquake and is represented as:

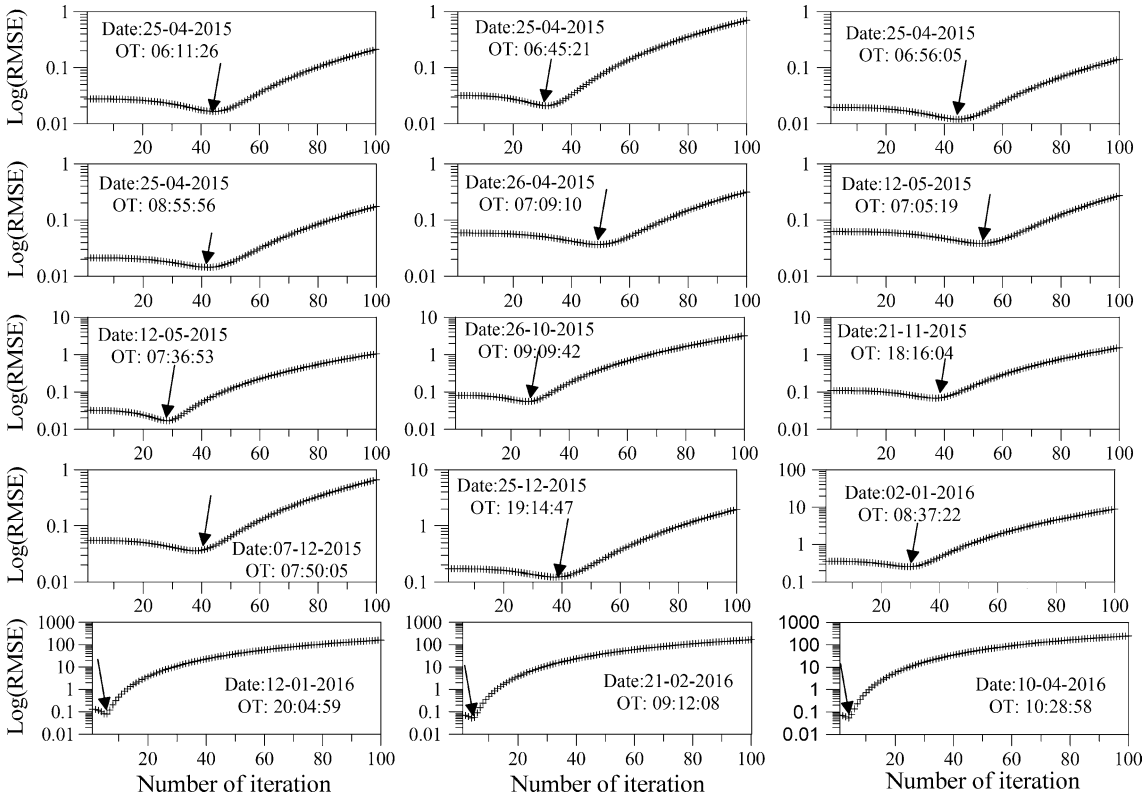

Fig. 5 Computed root mean square error (RMSE) at each iteration for different events recorded at Ghuttu station. *Arrow* indicates the number of iterations corresponding to minimum RMSE for each event

$$C = M_o R_{\theta\phi}.PRTITN.FS/(4\pi\rho\beta^3) \quad (9)$$

M_o, $R_{\theta\phi}$, FS and PRTITN are the seismic moment, radiation pattern, amplification caused by free surface and reduction factor, which accounts for partition of energy into two horizontal components, respectively. The term ρ and β are the density of the medium and the velocity of shear wave, respectively. The source spectrum of earthquake is represented by $S(f, f_c)$ which can be calculated as (Aki 1967 and Brune 1970):

$$S(f,f_c) = (2\pi f)^2/\left(1 + (f/f_c)^2\right) \quad (10)$$

where the term f_c represents the corner frequency of the spectrum. Equation (8) serves as a foundation of the present inversion algorithm which should be linearized to determine the unknown parameter. The natural logarithm of Eq. (8) linearizes it:

$$\ln A(f) = \ln C + \ln\left(S(f, f_c)\right) - \pi f R/Q_\beta(f)\beta - \ln(R) \quad (11)$$

Now, above equation is in linearized form where $Q_\beta(f)$ and f_c are unknown. The value of source spectra $S(f, f_c)$ can be replaced by Eq. (10). A number of possibilities of f_c are considered in this approach, and by taking different values of corner frequency, unknown parameter, i.e. $Q_\beta(f)$, is determined from inversion algorithm in least square sense:

$$\chi^2 = \sum \left[A_s(f) - S(f, f_c)\right]^2 \quad (12)$$

$S(f, f_c)$ and $A_s(f)$ are the theoretical source acceleration spectrum and source spectrum, respectively, and obtained from the inversion of Eq. (11). The final attenuation relation $Q_\beta(f) = 124f^{0.98}$ is obtained using the strong-motion data of NS and EW components of local earthquakes. The $Q_\beta(f)$ value obtained at different frequency is shown in Fig. 6a. The obtained $Q_\beta(f)$ relation suggests low values of 'Q_o' (<200) and high value of 'n' (>0.8) which revealed that the region is seismically active and characterized by local heterogeneities (Kumar et al. 2005b; Joshi 2006). The $Q_\beta(f)$ value obtained by using six earthquakes is quite reasonable as in the adjoining northern part of Kinnaur Himalaya region as the $Q_\beta(f) = 86 \pm 4f^{0.96\pm3}$ is obtained from local earthquake (Kumar et al. 2014a). Site amplification is obtained by residual of observed and theoretical source spectra as per Joshi (2006). To compute site amplification directly from the inversion scheme, the present algorithm is divided into two subinversion steps. The acceleration spectra without correction of site effect are considered as input of the first part of inversion scheme and outputs of this part

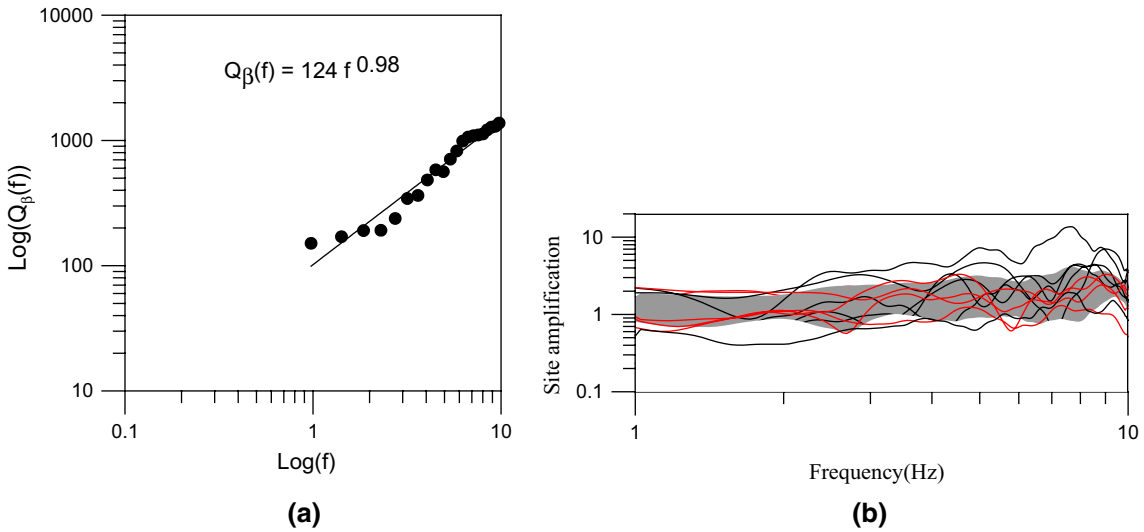

Fig. 6 **a** $Q_\beta(f)$ relationship obtained for site region. **b** Site effect at the recording station by using six local events. The *black* and *red lines* represent the site effects obtained by inversion for NS and EW component, respectively. The *shaded* area denotes the region between mean ± standard deviation

of inversion, i.e. M_o, f_c and $Q_\beta(f)$ are utilized to obtain residual of theoretical and observed source spectra, which is considered as site amplification. The obtained site amplification is utilized to correct acceleration spectrum, and this corrected spectrum is employed as input to the second part of inversion, and the final $Q_\beta(f)$ relation is obtained from the output of this second part of inversion algorithm. From local earthquakes, the site effects are obtained by using both the NS and EW components for the present study region and are shown in Fig. 6b.

Results and discussion

The source parameters of the devastating Gorkha Nepal earthquake of 25 April 2015, its large size aftershocks and recent earthquakes in Hindu kush region are obtained using the horizontal components of accelerograms recorded at MPGO, Ghuttu station. The epicentres of these events are at regional distance located between 600 and 1050 km (Fig. 1). The shear wave acceleration spectrum of entire S-phase is used, which is identified based on the earthquake origin time and preliminary locations extracted from USGS (Table 1). As the magnitude of the events is higher (>5.2), the signal-to-noise ratio too is high resulting clear record of S-phase. Visual inspection is used to identify the S-phase onset, and a time window of appropriate length of entire S-phase is selected for processing. The acceleration spectrum of the selected shear wave time window is processed as per Sharma and Wason (1994) to estimate earthquake source parameters. The anelastic attenuation factors and site effects estimated in the previous sections correct the spectrum. The corner frequency and the long-term flat level for spectrum of each earthquake are obtained using already mentioned grid search technique to evaluate source parameters.

Based on strong-motion data, no previous information of the attenuation characteristic is available for recording station. Therefore, the strong-motion data of local earthquakes recorded at Ghuttu station deduce $Q_\beta(f) = 124f^{0.98}$ by using inversion of data. In Fig. 6a, value of $Q_\beta(f)$ at each frequency is obtained by using average value of $Q_\beta(f)$ of NS and EW component, and this value is further used to correct the spectra for site region. The obtained $Q_\beta(f)$ value resembles the available attenuation characteristic of the surrounding Kinnaur region (Kumar et al. 2014a). The attenuation factor ($Q_\beta(f)$) is not available for source area of Nepal region, and therefore, the value of adjoining eastern region of Sikkim Himalaya is utilized. An extensive work has been performed based on strong-motion data by Nath et al. (2005) and Nath and Thingbaijam (2009) for the Sikkim Himalaya. They obtained $Q_\beta(f) = 167f^{0.47}$ for the Sikkim Himalaya region, which seems to be reasonable value for the source region of Nepal Himalaya. Similarly, the $Q_\beta(f) = 130f^{0.79}$ and $Q_\beta(f) = 500$ are used for the source region of Hindu kush which is proposed by Wu and Aki (1988) and Yu et al. (1995), respectively. The use of two different values of attenuation for source and receiver regions has been suggested by Joshi et al. (2014) while performing the similar work during the occurrence of M_w 6.9 Sikkim earthquake of 2011. Joshi et al. (2014) divided the wave propagation path between source and receiver

into two parts. The region close to the source is taken as hypocentral region (distance <100 km) and treated as the source zone, whereas the remaining part (hypocentral distance >100 km) is considered as site region as described in Eq. (7). This course of line is adopted to process whole data set, and the acceleration spectra are corrected for two different attenuation quality factors for source and site.

A numerical experiment is performed to check the effect of variable attenuation factors along with site effects on the source acceleration spectrum. This experiment is executed on NS component of Gorkha (M_w 7.8) earthquake. First, source acceleration spectrum is obtained by using the correction of anelastic attenuation for source region only and comparison is made with the theoretical Brune's spectrum. This spectrum is not correctly modelled with theoretical spectrum as shown in Fig. 7a. In the second step, spectrum is corrected for anelastic attenuation of site region only and again it is seen that it does not provide best match with theoretical spectrum as shown in Fig. 7b. In the next step, spectrum is corrected for both anelastic attenuation of source and site region and now it shows better match with theoretical spectrum (Fig. 7c) than the previous cases. In the last step, along with variable anelastic attenuation for source and site region, site effect also included for correcting the spectrum and it gives best match with the theoretical spectrum (Fig. 7d).

Similarly, another experiment is performed to validate the use of two separate Q_β values for the Hindu kush source region. A total of eight earthquakes of Hindu kush region are evaluated out of which seven events originated from intermediate focal depth (102–239 km) and one shallow focused event is located at 22 km focal depth. This shallow focused event is mainly located northeast of the Hindu kush region which is occurred within western part of the Tibetan plateau. The value $Q_\beta = 500$ is proposed by Yu et al. (1995) for seismic events deeper than 30 km for the Himalaya region, and this value is used for deep focused earthquakes of Hindu kush region. However, in case of single shallow focused event of this region the $Q_\beta(f) = 130f^{0.79}$ given by Wu and Aki (1988) is used. The acceleration spectrum is corrected by using two different Q_β values as $Q_\beta(f) = 130f^{0.79}$ for shallow focused earthquakes and $Q_\beta = 500$ for deeper earthquakes. Analysis performed for two events, M_w 7.5 intermediate focal depth of 231 km and M_w 7.2 shallow focused of 22 km depth, has been assessed, and results are plotted in Fig. 8. First, the spectrum of the event with M_w 7.5 is corrected for anelastic attenuation by using $Q_\beta(f) = 130f^{0.79}$, and in the second step it is evaluated using $Q_\beta = 500$. In both cases, the results are compared with theoretical Brune's spectrum, which are plotted in Fig. 8a, b, respectively. It clearly indicates that better match is attained between observed and theoretical spectrum for $Q_\beta = 500$. Similarly, both values, i.e. $Q_\beta(f) = 130f^{0.79}$ and $Q_\beta = 500$, are used to correct the spectrum of M_w 7.2 event and comparison is made with theoretical spectrum as shown in Fig. 8c, d, respectively. In this case, the spectrum gives better match for $Q_\beta(f) = 130f^{0.79}$ (Fig. 8c). Therefore, utilization of two separate Q_β values for shallow focused and intermediate focused earthquakes is required for the Hindu kush region. The evaluated corrected source acceleration spectra of the NS component of all events are plotted in Fig. 9 along with Brune's theoretical spectra. The similar estimations for the EW component for all these events are shown in Fig. 10. Overall comparison of theoretical spectra matches well with the estimated values; however, results are more favourable for high-frequency record which is also earlier reported by Joshi et al. (2014).

The seismic moment is equivalent to the size of the rupture zone, and it is calculated using Eq. 4 (Brune 1970, 1971). In this relation, the values of density (ρ) and shear wave velocity (β) are taken as 2700 kg/m^3 and 3.5 km/s

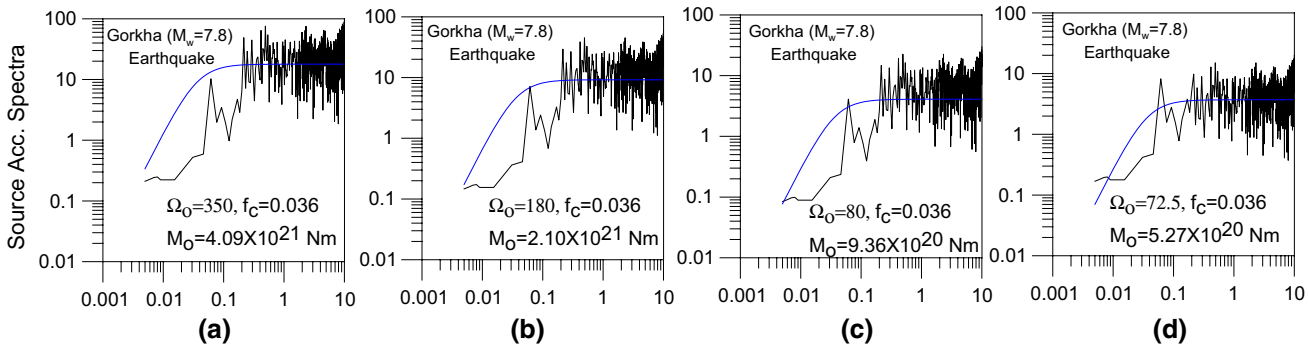

Fig. 7 Comparison of observed and theoretical spectra of NS component of Gorkha (M_w 7.8) earthquake using correction of **a** anelastic attenuation ($Q_\beta(f)$) for source region only, **b** $Q_\beta(f)$ for site region only, **c** both $Q_\beta(f)$ for source and site regions and **d** using both $Q_\beta(f)$ for source and site regions along with the site amplification term. The *blue* and *black colours* denote theoretical and observed spectrum, respectively

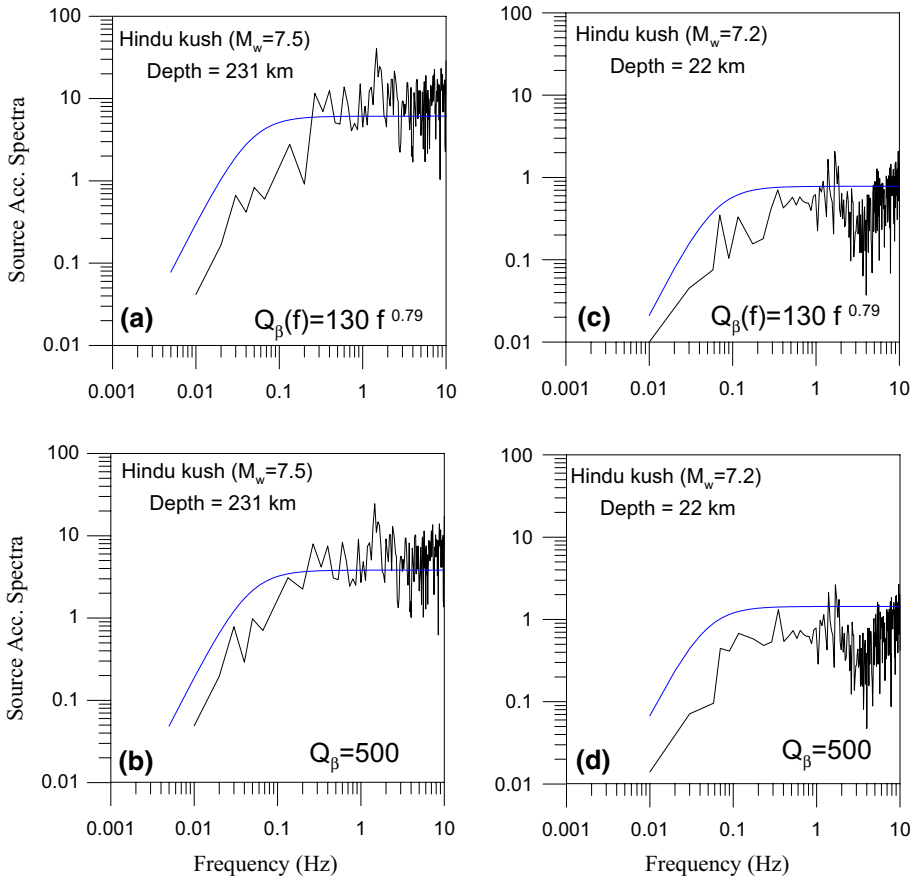

Fig. 8 Comparison of observed and theoretical spectra of NS component of Hindu kush (M_w 7.5) earthquake using correction of two different values of anelastic attenuation as **a** $Q_\beta(f) = 130f^{0.79}$ and **b** $Q_\beta = 500$. Similar comparison for another Hindu kush event of M_w 7.2 using correction of anelastic attenuation as **c** $Q_\beta(f) = 130f^{0.79}$ and **d** $Q_\beta = 500$. The *blue* and *black colours* denote theoretical and observed spectrum, respectively

(Joshi et al. 2014). The radius of the circular source is estimated using Eq. (5) where f_c is the corner frequency of the spectrum. A decrease in stress level over the fault plane as an average difference of stress level before and after the occurrence of earthquake is described as the stress drop. The evaluated seismic moment and the source radius are related to the stress drop as proposed by Papageorgiou and Aki (1983). The calculated parameters of the present data set are given in Table 2. Using the above-mentioned method, the average value of the seismic moment obtained by using NS and EW components of M_w 7.8 Nepal earthquake is 5.72×10^{20} Nm while its value given by USGS and Harvard CMT solution is 6.62×10^{20} and 8.39×10^{20} Nm, respectively. In Fig. 11, a comparison is made between obtained values of seismic moment for different earthquakes and the seismic moment given by USGS and CMT Harvard. Comparison reveals a close resemblance of each evaluated value with previous estimates by other agencies.

The stress drop values computed for various earthquakes in this work lie within the range of stress drop value computed for Himalaya region by different workers. The average stress drop obtained for Gorkha earthquake is 50.6 bar, and its value given by Mitra et al. (2015) is 34 ± 3.79 bar. The stress drop measured during the occurrence of M_w 6.9 Sikkim earthquake of 2011 by Joshi et al. (2014) is 59.2 ± 8.8 bar, and the epicentre of this event is in the Sikkim Himalaya located towards east from the recent Gorkha earthquake. In the western part of Garhwal Himalaya, the stress drop measured during M_s 7.0 Uttarkashi earthquake of 1991 and M_s 6.6 Chamoli earthquake of 1999 is 53 and 65 bars, respectively (Kumar et al. 2005a). The average stress drop estimated for various earthquakes in the present study varies between 7.1 and 50.6 bar. These low values of stress drop are well quantified for interplate zones such as Himalaya which are already verified earlier for different parts of the India–Eurasia collision (Kumar et al. 2005a, 2013a; Joshi et al. 2014; Mitra et al. 2015). Physical hypothesis of Brune's circular model suggests that the stress drop for one particular geotectonic regime is required to be constant irrespective of its release during the occurrence of any magnitude size or rupture dimension of the

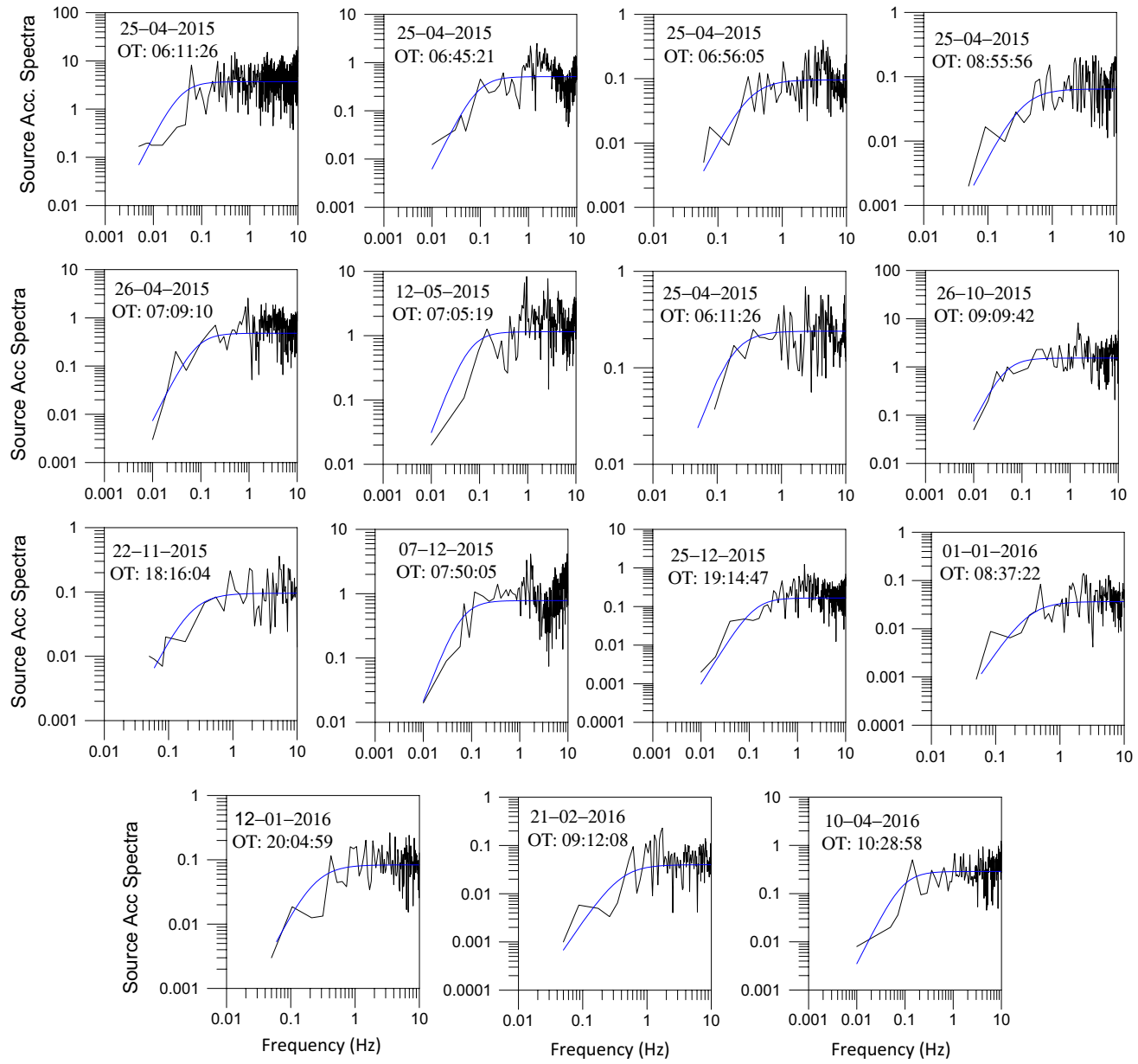

Fig. 9 Source acceleration spectra of NS component of all events used in this work along with theoretical Brune's (1970) spectra. The *black* and *blue lines* denote the observed spectra and theoretical spectra, respectively

earthquake. The obtained stress drop for the present data set is variable, and its value increases with the increase in event size. Lorenzo et al. (2010) and Kumar et al. (2013a) have explained that this type of variation in stress drop within one particular seismic regime is governed by self-similar behaviour of earthquake sources.

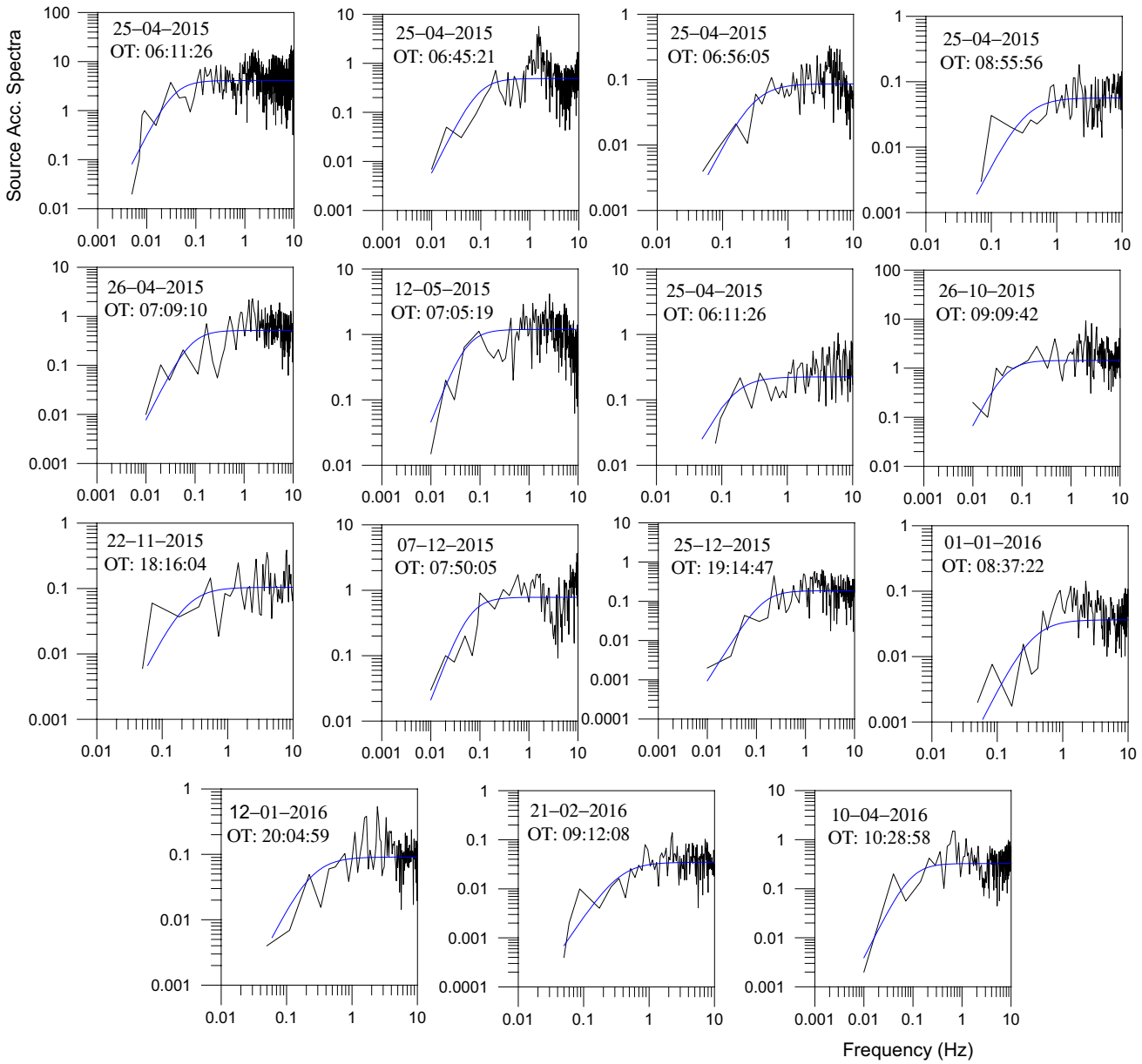

Fig. 10 Source acceleration spectra of EW component of all events used in this work along with theoretical Brune's (1970) spectra. The *black* and *blue lines* denote the observed spectra and theoretical spectra, respectively

Conclusions

In the present work, the source parameters of M_w 7.8 Gorkha Nepal earthquake of 25 April 2015, its six large aftershocks and earthquakes originate in Hindu kush region including M_w 7.5 major earthquake of 26 October 2015 are reported. Estimation is performed using strong-motion data recorded at the epicentre distance range of 600–1050 km. Numerical methodology is carried out to evaluate source parameters for the recent major and higher magnitude events of Nepal Himalaya and Hindu kush regions, in which the effects of variable anelastic attenuation and site effects are isolated from shear wave spectra. The evaluated seismic moment of the Gorkha (M_w 7.8) and Hindu kush

Table 2 Source parameters obtained from NS and EW component of the events

Event Date (dd-mm-yyyy) Origin time (hh:mm:s)		Corner freq. (Hz)	Seismic moment (Nm)	Average seismic moment (Nm)	Stress drop (bars)	Average stress drop (bars)	Source radius (km)	Average source radius (km)
25-04-2015	EW	0.035	6.17×10^{20}	5.72×10^{20}	52.5	50.60	37.2	36.70
06:11:26	NS	0.036	5.27×10^{20}		48.7		36.2	
25-04-2015	EW	0.091	1.12×10^{19}	1.15×10^{19}	16.7	16.95	14.3	14.35
06:45:21	NS	0.090	1.19×10^{19}		17.2		14.4	
25-04-2015	EW	0.29	2.19×10^{17}	2.23×10^{17}	10.6	11.40	4.5	4.40
06:56:05	NS	0.30	2.28×10^{17}		12.2		4.3	
25-04-2015	EW	0.32	1.16×10^{17}	1.20×10^{17}	7.5	8.15	4.1	4.0
08:55:56	NS	0.33	1.24×10^{17}		8.8		3.9	
26-04-2015	EW	0.081	1.77×10^{19}	1.72×10^{19}	18.7	17.90	16.1	16.20
07:09:10	NS	0.080	1.68×10^{19}		17.1		16.3	
12-05-2015	EW	0.05	1.08×10^{20}	9.01×10^{19}	26.7	28.80	26.1	23.90
07:05:19	NS	0.06	7.23×10^{19}		30.9		21.7	
12-05-2015	EW	0.14	2.63×10^{18}	2.54×10^{18}	14.3	15.35	9.3	9.0
07:36:53	NS	0.15	2.45×10^{18}		16.4		8.7	
25-10-2015	EW	0.045	2.18×10^{20}	2.30×10^{20}	39.3	40.05	28.9	29.25
09:09:42	NS	0.044	2.41×10^{20}		40.8		29.6	
22-11-2015	EW	0.23	5.47×10^{17}	5.47×10^{17}	13.2	12.35	5.7	5.80
18:16:04	NS	0.22	5.47×10^{17}		11.5		5.9	
07-12-2015	EW	0.060	6.42×10^{19}	6.72×10^{19}	27.6	30.40	21.7	21.35
07:50:05	NS	0.062	7.02×10^{19}		33.2		21.0	
25-12-2015	EW	0.14	2.74×10^{18}	2.80×10^{18}	14.9	13.65	9.3	9.65
19:14:47	NS	0.13	2.85×10^{18}		12.4		10.0	
02-01-2016	EW	0.34	9.25×10^{16}	9.53×10^{16}	7.2	7.10	3.8	3.85
08:37:22	NS	0.33	9.82×10^{16}		7.0		3.9	
12-01-2016	EW	0.24	4.68×10^{17}	4.68×10^{17}	12.8	12.05	5.4	5.55
20:04:59	NS	0.23	4.68×10^{17}		11.3		5.7	
21-02-2016	EW	0.35	8.31×10^{16}	8.20×10^{16}	7.0	7.90	3.7	3.55
09:12:08	NS	0.38	8.08×10^{16}		8.8		3.4	
10-04-2016	EW	0.091	1.14×10^{17}	1.09×10^{17}	17.0	15.90	14.3	14.35
10:28:58	NS	0.090	1.03×10^{17}		14.8		14.4	

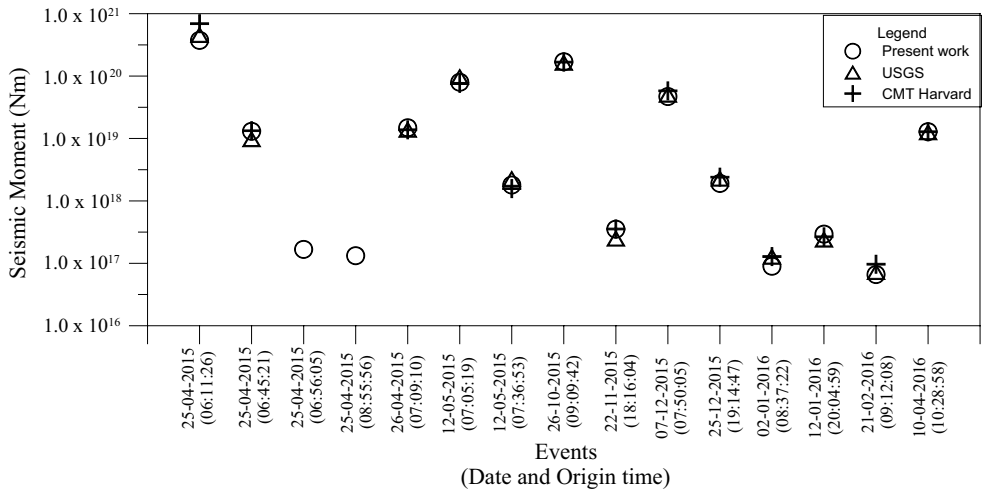

Fig. 11 Comparison of obtained seismic moment of all evaluated seismic events along with the available seismic moment given by different agencies

(M_w 7.5) earthquakes is 5.72 × 10^{20} and 2.30 × 10^{20} Nm, respectively, and it varies between 8.20 × 10^{16} and 9.01 × 10^{19} Nm for other earthquakes of M_w magnitude range between 5.2 and 7.3 in this work. These values are in agreement with USGS and others reports which suggest that variable anelastic attenuation should be used for different zones of wave propagation path. The source radius for these events based on the Brune's circular model is in the range of 3.55–36.70 km. The average stress drop evaluated for these events is in the range of 7.1–50.6 bars which is within the well-established range of the interplate region.

Acknowledgements We thank the Director, WIHG, Dehradun, for giving permission to publish this work. The MPGO-EPR team of WIHG is thankworthy for collecting strong-motion data through a Ministry of Earth Sciences (MoES), New Delhi, sponsored project (MoES/P.O. (Seismo)/NPEP(15)/2009). The earthquakes information obtained from the official websites of Indian Meteorological Department (IMD) and United States Geological Survey (USGS) is thankfully acknowledged. Associated Editor: S. Mukherjee, Managing Editor: Monika Dullo, Chief Editor: W.C Dullo and two anonymous reviewers are highly acknowledged for constructive suggestions and critical review.

References

Aki K (1967) Scaling law of seismic spectrum. J Geophys Res 72:1217–1231

Ali SM, Shanker D (2016) Study of seismicity in the NW Himalaya and adjoining regions using IMS network. J Seismol. doi:10.1007/s10950-016-9603-7

Atkinson GM, Boore DM (1995) Ground-motion relation for eastern North America. Bull Seismol Soc Am 85:17–30

Atkinson GM, Boore DM (1998) Evaluation of models for earthquake source spectra in eastern North America. Bull Seismol Soc Am 88:917–934

Bilham R (2015) Raising Kathmandu. Nat Geosci 8:582–585

Boore DM (1983) Stochastic simulation of high-frequency ground motions based on seismological models of the radiated spectra. Bull Seismol Soc Am 73:1865–1894

Boore DM, Atkinson G (1987) Stochastic prediction of ground motion and spectral response parameters at hard-rock sites in eastern North America. Bull Seismol Soc Am 73:1865–1894

Boore DM, Bommer J (2005) Processing of strong motion accelerograms: needs, options and consequences. Soil Dyn Earthq Eng 25:93–115

Brune JM (1970) Tectonic stress and spectra of seismic shear waves from earthquakes. J Geophys Res 75:4997–5009

Brune JM (1971) Correction. J Geophys Res 76:5002

Chatelain JL, Roecker SW, Hatzfeld D, Molnar P (1980) Microearthquake seismicity and fault plane solutions in the Hindukush region and their tectonic implications. J Geophys Res 85(B3):1365–1387

Elliott JR, Jolivet R, Gonzalez PJ, Avouac JP, Hollingsworth J, Searle MP, Stevens VL (2016) Himalayan megathrust geometry and relation to topography revealed by the Gorkha earthquake. Nat Geosci 6:174–184

Fletcher JB (1980) Spectra from high dynamic range digital recordings at Oroville, California aftershocks and their source parameters. Bull Seismol Soc Am 70:735–755

Fletcher JB (1982) A comparison between the tectonic stress measured in situ and stress parameters from induced seismicity at Monticello reservoir, South Carolina. J Geophys Res 87:6931–6944

Hadley DM, Helmberger DV, Orcutt JA (1982) Peak ground acceleration scaling studies. Bull Seismol Soc Am 72:959–978

Hanks TC (1977) Earthquake stress drops, ambient tectonic stresses and stresses that drive plate motions. Pure Appl Geophys 115:441–458

Hanks TC, Kanamori H (1979) A moment magnitude scale. J Geophys Res 84(B5):2348–2350

Irikura K (1983) Semi empirical estimation of strong ground motion during large earthquakes. Bull Disaster Prev Res Inst 33:63–104

Islam R, Thakur VC (1998) Geology of Bhilangna valley, Garhwal Himalaya. Geosci J 9(2):143–152

Jain AK (2014) When did India-Asia collide and make the Himalaya? Curr Sci 106(2):254–266

Joshi A (2006) Use of acceleration spectra for determining the frequency dependent attenuation coefficient and source parameters. Bull Seismol Soc Am 96:2165–2180

Joshi A, Kumar P, Mohanty M, Bansal AR, Dimri VP, Chadha RK (2012) Determination of $Q_{\beta}(f)$ at different places of Kumaon Himalaya from the inversion of spectral acceleration data. Pure Appl Geophys 169:1821–1845

Joshi A, Kumar P, Arora S (2014) Use of site amplification and anelastic attenuation for the determination of source parameters of the Sikkim earthquake of September 18, 2011, using far-field strong-motion data. Nat Hazards 70:217–235

Kanamori H (1979) A semi empirical approach to prediction of long period ground motions from great earthquakes. Bull Seismol Soc Am 69:1645–1670

Kumar N, Khandelwal D (2015) Strong motion data analysis of the 4 April 2011 Western Nepal earthquake (M 5.7) and its implications to the seismic hazard in the Central Himalaya. Curr Sci 109(10):1822–1830

Kumar D, Sarkar I, Sri Ram V, Khattri KN (2005a) Estimation of the source parameters of the Himalaya earthquake of October 19, 1991, average effective shear wave attenuation parameter and local site effects from accelerograms. Tectonophysics 407:1–24

Kumar N, Parvez IA, Virk HS (2005b) Estimation of coda wave attenuation for NW Himalayan region using local earthquakes. Phys Earth Planet Inter 151:243–258

Kumar N, Yadav DK, Mondal SK, Roy PNS (2013a) Stress drop and its relation to tectonic and structural elements for the meizoseismal region of great 1905 Kangra earthquake of the NW Himalaya. Nat Hazards 69(3):2021–2038

Kumar P, Joshi A, Verma OP (2013b) Attenuation tomography based on strong motion data: case study of central Honshu region, Japan. Pure Appl Geophys 170:2087–2106

Kumar N, Mate S, Mukhopadhyay S (2014a) Estimation of Qp and Qs of Kinnaur Himalaya. J Seismol 18:47–59

Kumar P, Joshi A, Arora S, Kumar A (2014b) Three-dimensional attenuation structure in the region of Kumaon Himalaya, India based on inversion of strong motion data. Pure Appl Geophys 172:333–358

Kumar P, Joshi A, Sandeep Kumar A, Chadha RK (2015) Detailed attenuation study of shear waves in the Kumaon Himalaya, India, using the inversion of strong-motion data. Bull Seismol Soc Am 105(4):1836–1851

Lorenzo SD, Zollo A, Zito G (2010) Source, attenuation, and site parameters of the 1997 Umbria-Marche seismic sequence from the inversion of P wave spectra: a comparison between constant Q_P and frequency-dependent Q_P models. J Geophys Res 115:B09306. doi:10.1029/2009JB007004

Mitra S, Paul H, Kumar A, Singh SK, Dey S, Powali D (2015) The 25 April 2015 Nepal earthquake and its aftershocks. Curr Sci 108:1938–1943

Mukherjee S (2005) Channel flow, ductile extrusion and exhumation of lower-mid crust in continental collisional zones. Curr Sci 89:435–436

Mukherjee S (2013) Channel flow extrusion model to constrain dynamic viscosity and Prandtl number of the Higher Himalayan Shear Zone. Int J Earth Sci 102:1811–1835

Mukherjee S, Koyi HA (2010) Higher Himalayan Shear Zone, Sutlej section: Structural geology & extrusion mechanism by various combinations of simple shear, pure shear & channel flow in shifting modes. Int J Earth Sci 99:1267–1303

Mukherjee S, Mukherjee B, Thiede R (2013) Geosciences of the Himalaya-Karakoram-Tibet Orogen. Int J Earth Sci 102:1757–1758

Mukherjee S, Carosi R, van der Beek PA, Mukherjee BK, Robinson DM (2015) Tectonics of the Himalaya: an introduction. Geol Soc Lond Spec Publ 412:1–3

Muller RD (2010) Tectonics: sinking continents. Nat Geosci 3:79–80

Nath SK, Thingbaijam KKS (2009) Seismic hazard assessment—a holistic microzonation approach. Nat Hazards Earth Syst Sci 9:1445–1459

Nath SK, Vyas M, Pal I, Singh AK, Mukherjee S, Sengupta P (2005) Spectral attenuation models in the Sikkim Himalaya from the observed and simulated strong motion events in the region. Curr Sci 88(2):295–303

Papageorgiou A, Aki K (1983) A specific barrier model for the quantitative description of inhomogeneous faulting and the prediction of strong ground motion. Part 1. Description of the model. Bull Seismol Soc Am 73:693–722

Pavlis GL (2000) The Pamir-Hindu Kush seismic zone as a strain marker for flow in the upper mantle. Tectonics 19(1):103–115

Roecker SW, Soboleva OV, Nersesov IL, Lukk AA, Hatzfeld D, Chatelain JL, Molnar P (1980) Seismicity and fault plane solutions of intermediate depth earthquakes in the Pamir-Hindukush region. J Geophys Res 85(B3):1358–1364

Ruff LJ (1999) Dynamic stress drop of recent earthquakes: variations within subduction zones. Pure Appl Geophys 154:409–431

Sharma ML, Wason HR (1994) Occurrence of low stress drop earthquakes in the Garhwal Himalaya region. Phys Earth Planet Inter 34:159–172

Valdiya KS (1980) Geology of the Kumaon Lesser Himalaya. Wadia Institute of Himalayan Geology, Dehradun, p 291

Vyshnavi S, Islam R, Sundriyal YP (2014) Comparative study of soil profiles developed on metavolcanic (basaltic) rocks in two different watersheds of Garhwal Himalaya. Curr Sci 108(4):699–707

Whipple KX, Shirzaei M, Hodges KP, Arrowsmith JR (2016) Active shortening within the Himalayan orogenic wedge implied by the 2015 Gorkha earthquake. Nat Geosci 9:711–718

Wu R, Aki K (1988) Multiple scattering and energy transfer of seismic waves—separation of scattering effect from intrinsic attenuation II. Application of the theory to Hindu Kush region. Pure Appl Geophys 128(1):49–80

Yadav RBS, Tsapanos TM, Bayrak Y, Koravos GC, Devlioti KD (2013) Spatial mapping of earthquake hazard parameters in the Hindukush-Pamir Himalaya and adjacent regions: implication for future seismic hazard. J Asian Earth Sci 70–71:115–124

Yin A (2006) Cenozoic tectonic evolution of the Himalayan orogen as constrained by along-strike variation of structural geometry, exhumation history, and foreland sedimentation. Earth Sci Rev 76:1–131

Yu G, Khattri KN, Anderson JG, Brune JN, Zeng Y (1995) Strong ground motion from the Uttarkashi earthquake, Himalaya, India, earthquake: comparison of observations with synthetics using the composite source model. Bull Seismol Soc Am 85:31–50